

Particle–Interface Interaction across a Nonpolar Medium in Relation to the Production of Particle-Stabilized Emulsions

K. D. Danov,[†] P. A. Kralchevsky,^{*,†} K. P. Ananthapadmanabhan,[§] and A. Lips[§]

Laboratory of Chemical Physics & Engineering, Faculty of Chemistry, University of Sofia, 1164 Sofia, Bulgaria, and Unilever Research & Development, Trumbull, Connecticut 06611

Received September 15, 2005. In Final Form: October 16, 2005

Quantitative theory of the particle–interface interaction across a nonpolar medium is developed. We consider a spherical dielectric particle (phase 1), which is immersed in a nonpolar medium (phase 2), near its boundary with a third dielectric medium (phase 3). The interaction originates from electric charges at the particle surface (e.g., the surface of a silica particle immersed in oil). The theoretical problem is solved exactly, in terms of Legendre polynomials, for arbitrary values of the dielectric constants of the three phases. As a result, expressions for calculating the interaction force and energy are derived. These expressions generalize the known theory of the electrostatic image force (acting on point charges) to the case of particles that have finite size and uniform surface charge density. For typical parameter values (silica or glass particles immersed in tetradecane), the image–force interaction becomes significant for particles of radius $R > 30$ nm. At fixed relative particle-to-interface distance, the force increases with the cube of the particle radius. In general, this is a strong and long-range interaction. For micrometer-sized particles, the interaction energy could be on the order of $10^5 k_B T$ at close contact, and, in addition, the interaction range could be about 10^5 particle radii. The sign of the interaction depends on the difference between the dielectric constants of phases 2 and 3. When phase 3 has a smaller dielectric constant (e.g., air), the interface repels the particle. In contrast, when phase 3 has a greater dielectric constant (e.g., water), the interaction is attractive. Especially, water drops attract charged hydrophobic particles dispersed in the oily phase, and thus favor the formation of reverse particle-stabilized (Pickering) emulsions. The particle–interface interaction across the oily phase is insensitive to the concentration of electrolyte in the third, aqueous phase.

1. Introduction

Adsorption layers of colloidal particles play a central role in the formation of Pickering emulsions.^{1–7} If the particle adsorption is fast enough, the newly formed emulsion drops will not coalesce upon collision, and a fine emulsion will be produced. In contrast, if the particle adsorption occurs slowly, the collision of bare drops (unprotected by particle monolayers) would lead to drop coalescence and eventually to phase separation.⁸

When the particles are dispersed in the *water* phase, it often happens that the emulsion drops and the particles bear surface electric charges of the same sign. Then, the overlap of the electric double layers around the particles and drops gives rise to a strong double-layer repulsion between them. It is known that the bare oil–water interface is negatively charged because of the adsorption of OH^- ions.⁹ Therefore, any kind of negatively charged

particles will be repelled by the drops (Figure 1a). In such a case, adsorption is possible only if the electrostatic barrier is overcome (because of the mechanical energy of agitation), or suppressed by the addition of electrolyte. The experiment indicates that the addition of electrolyte facilitates the formation of oil-in-water emulsions,^{10,11} although the effect of the ionic strength is more complex because of the occurrence of particle flocculation in the aqueous phase.^{5,10,11}

The situation can be quite different if the particles have been initially dispersed in the *oily* phase. A number of experimental studies indicate that electric charges can be present at the particle–oil boundary.^{12–19} If such is the case, the particles will be attracted

* Corresponding author. Phone: (+359) 2-962 5310. Fax: (+359) 2-962 5438. E-mail: pk@lcpe.uni-sofia.bg.

[†] University of Sofia.

[§] Unilever Research & Development.

(1) Pickering, S. U. Emulsions. *J. Chem. Soc.* **1907**, 91, 2001–2021.

(2) Tambe, D. E.; Sharma, M. M. The effect of colloidal particles on fluid–fluid interfacial properties and emulsion stability. *Adv. Colloid Interface Sci.* **1994**, 52, 1–63.

(3) Thieme, J.; Abend, S.; Lagaly, G. Aggregation in Pickering emulsions. *Colloid Polym. Sci.* **1999**, 277, 257–260.

(4) Binks, B. P. Particles as surfactants – similarities and differences. *Curr. Opin. Colloid Interface Sci.* **2002**, 7, 21–41.

(5) Aveyard, R.; Binks, B. P.; Clint, J. H. Emulsions stabilized solely by colloidal particles. *Adv. Colloid Interface Sci.* **2003**, 100–102, 503–546.

(6) Nushtaeva, A. V.; Kruglyakov, P. M. Capillary pressure in thinning emulsion film stabilized with solid particles. *Colloid J.* **2003**, 65, 341–349.

(7) Arditty, S.; Whitby, C. P.; Binks, B. P.; Schmitt, V.; Leal-Calderon, F. Some general features of limited coalescence in solid-stabilized emulsions. *Euro. Phys. J. E* **2003**, 11, 273–281.

(8) Kralchevsky, P. A.; Ivanov, I. B.; Ananthapadmanabhan, K. P.; Lips, A. On the Thermodynamics of Particle-Stabilized Emulsions: Curvature Effects and Catastrophic Phase Inversion. *Langmuir* **2005**, 21, 50–63.

(9) Marinova, K. G.; Alargova, R. G.; Denkov, N. D.; Velez, O. D.; Petsev, D. N.; Ivanov, I. B.; Borwankar, R. P. Charging of Oil–Water Interfaces Due to Spontaneous Adsorption of Hydroxyl Ions. *Langmuir* **1996**, 12, 2045–2051.

(10) Binks, B. P.; Lumsdon, S. O. Stabilization of oil-in-water emulsions stabilized by silica particles. *Phys. Chem. Chem. Phys.* **1999**, 1, 3007–3016.

(11) Ashby, N. P.; Binks, B. P. Pickering emulsions stabilized by Laponite clay particles. *Phys. Chem. Chem. Phys.* **2000**, 2, 5640–5646.

(12) Aveyard, R.; Clint, J. H.; Nees, D.; Paunov, V. N. Compression and Structure of Monolayers of Charged Latex Particles at Air/Water and Octane/Water Interfaces. *Langmuir* **2000**, 16, 1969–1979.

(13) Aveyard, R.; Binks, B. P.; Clint, J. H.; Fletcher, P. D. I.; Horozov, T. S.; Neumann, B.; Paunov, V. N.; Annesley, J.; Botchway, S. W.; Nees, D.; Parker, A. W.; Ward, A. D.; Burgess, A. N. Measurement of long-range repulsive forces between charged particles at an oil–water interface. *Phys. Rev. Lett.* **2002**, 88, 246102.

(14) Horozov, T. S.; Aveyard, R.; Clint, J. H.; Binks, B. P. Order–Disorder Transition in Monolayers of Modified Monodisperse Silica Particles at the Octane–Water Interface. *Langmuir* **2003**, 19, 2822–2829.

(15) Stancik E. J.; Kouhkan, M.; Fuller, G. G. Coalescence of Particle-Laden Fluid Interfaces. *Langmuir* **2004**, 20, 90–94.

(16) Danov, K. D.; Kralchevsky, P. A.; Boneva, M. P. Electrostatic Force Acting on Solid Particles at a Fluid Interface. *Langmuir* **2004**, 20, 6139–6151.

(17) Horozov, T. S.; Aveyard, R.; Clint, J. H. Particle Zips: Vertical Emulsion Films with Particle Monolayers at their Surfaces. *Langmuir* **2005**, 21, 2330–2341.

(18) Horozov, T. S.; Aveyard, R.; Binks, B. P.; Clint, J. H. Structure and Stability of Silica Particle Monolayers at Horizontal and Vertical Octane–Water Interfaces. *Langmuir* **2005**, 21, 7407–7412.

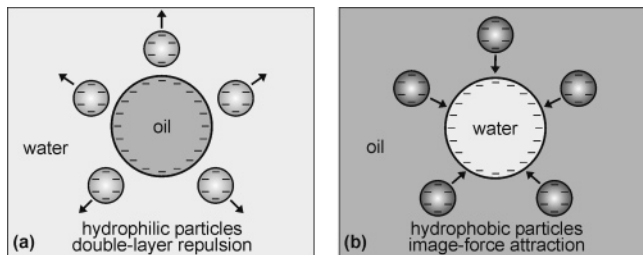


Figure 1. (a) The double-layer repulsion between like-charged colloidal particles and oil drops in water medium impedes the particle adsorption at the oil–water interface. (b) When particles dispersed in the oil bear surface electric charges, they are attracted by the water drops because of the image-force effect (see eq 2.25).

by the oil–water interface, as proven in the present paper. Physically, this effect is related to the electrostatic image force.^{20,21} The respective energy of electrostatic attraction is much greater than the thermal energy, $k_B T$ (k_B – Boltzmann constant; T – temperature). This attraction is able to cause quick particle adsorption at the surfaces of the newly formed emulsion drops (Figure 1b) to protect the latter against coalescence and to favor the formation of fine reverse emulsions. Analogous force that pushes the particle into the water (electrodipping force) is experienced also by the particles, which are attached to the oil–water interface and form a finite contact angle.¹⁶

The interaction between a charged particle in oil and the oil–water interface has been theoretically described only in the case of a point particle (charge): this is the conventional image force.^{20,21} Here, our aim is to develop a quantitative theory of the particle–interface interaction in the case of a spherical particle of finite size that bears electric charge of a given surface density. The problem is formulated and solved in the general case, where the particle and the two large phases have different dielectric constants. The interaction of a dielectric particle with an oil–water or oil–air interface represents a special case of the considered problem.

The paper is organized as follows: In section 2, we solve the electrostatic problem and derive equations for the electrostatic potential and the interaction force and energy. In section 3, we consider the special case when the particle has the same dielectric constant as the surrounding nonpolar phase (oil); then, the theoretical expressions are much simpler. In addition, we examine the effect of electrolyte concentration in the aqueous phase. Section 4 is focused on the procedure for the computation of the interaction force and energy. Illustrative numerical results are reported and discussed in section 5. In Appendix A, it is demonstrated that the effect of electrolyte concentration in the water phase is rather weak. Appendices B and C, containing parts of the theoretical derivations, are given as Supporting Information.

2. Electric Field and Interaction Force

2.1. Electric Potential in the Three Phases. We consider a spherical particle (dielectric phase 1), of radius R , that is immersed in another dielectric phase 2. The particle is situated at a surface-to-surface distance s to the flat interface between phases 2 and 3 (Figure 2). We assume that phase 3 is also dielectric, but, as

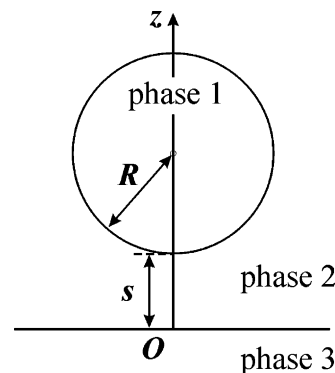


Figure 2. Sketch of a particle of radius, R , which is immersed in phase 2 and situated at a distance, s , to the boundary of phases 2 and 3. The three phases are dielectrics of constants ϵ_1 , ϵ_2 , and ϵ_3 , respectively.

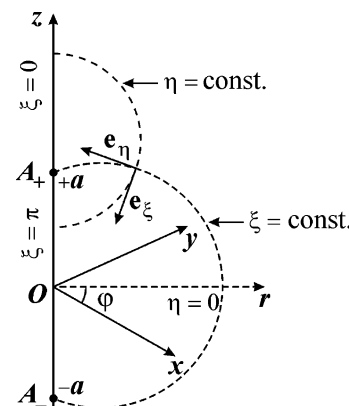


Figure 3. Sketch of the coordinate systems used: Cartesian coordinates (x, y, z) ; cylindrical coordinates (r, φ, z) , and bipolar coordinates (ξ, η, φ) with unit coordinate vectors \mathbf{e}_ξ and \mathbf{e}_η , and poles A_+ and A_- .

discussed in section 3.2, it could be also an aqueous phase that may contain dissolved electrolyte. In the case of reverse emulsions (Figure 1b), phase 2 is oil, whereas phase 3 is water. The dielectric constants of the three phases are denoted ϵ_1 , ϵ_2 , and ϵ_3 , respectively.

We assume that the charge density, σ , at the particle surface (the phase boundary between phases 1 and 2) is a known constant, whereas the interface between phases 2 and 3 is not charged. (If phase 3 is an aqueous electrolyte solution, the phase boundary 2–3 could bare surface electric charge, but the latter does not affect the particle–interface interaction; see section 3.2 and Appendix A). The total surface charge of the particle, Q , is

$$Q = 4\pi R^2 \sigma \tag{2.1}$$

The plane xy of the Cartesian coordinate system used (x, y, z) coincides with the boundary between phases 2 and 3; the z -axis is chosen to be the axis of rotational symmetry of the system (Figure 2). It is convenient to also introduce an auxiliary cylindrical coordinate system (r, φ, z) with radial coordinate r and polar angle φ :

$$x = r \cos \varphi, y = r \sin \varphi \tag{2.2}$$

However, the natural symmetry of the problem suggests introducing a bispherical (bipolar) coordinate system (ξ, η, φ) (see Figure 3), in which \mathbf{e}_ξ and \mathbf{e}_η denote the unit vectors along the respective coordinate lines. All ξ -lines are passing through the poles A_+ and A_- of the bipolar coordinate system, which are situated symmetrically with respect to the plane $z = 0$. The

(19) Horozov, T. S.; Binks, B. P. Particle behavior at horizontal and vertical fluid interfaces. *Colloids Surf. A* **2005**, *267*, 64–73.

(20) Landau, L. D.; Lifshitz, E. M. *Electrodynamics of Continuous Medium*; Pergamon Press: Oxford, U.K., 1960.

(21) Israelachvili, J. N. *Intermolecular and Surface Forces*; Academic Press: London, 1992.

coordinates of the poles A_{\pm} are $(0, 0, \pm a)$. The bipolar coordinates are defined as follows:^{22,23}

$$r = \frac{a}{h} \sin \xi, z = \frac{a}{h} \sinh \eta, h \equiv \cosh \eta - \cos \xi \quad (2.3)$$

where h is a metric coefficient. The Lamé coefficients of the bipolar coordinate system, h_{ξ} , h_{η} , and h_{φ} , are^{22,23}

$$h_{\xi} = h_{\eta} = \frac{a}{h}, h_{\varphi} = \frac{a}{h} \sin \xi \quad (2.4)$$

The upper part of the axis of revolution ($z > a$) corresponds to $\xi = 0$, whereas its lower part ($0 < z < a$) corresponds to $\xi = \pi$. The boundary between phases 2 and 3 (the plane $z = 0$) corresponds to $\eta = 0$. For the poles A_{\pm} , we have $\eta \rightarrow \pm\infty$. The coordinate surfaces of constant η are spheres:²³

$$r^2 + (z - a \coth \eta)^2 = \frac{a^2}{\sinh^2 \eta} \quad (2.5)$$

Equation 2.5 shows that the bipolar coordinate system can be chosen in such a way that the particle surface corresponds to a fixed η , viz. $\eta = \eta_s$. Then, the parameters a and η_s are related to the radius, R , and the distance, s (Figure 2), by the following expressions:

$$R + s = a \coth \eta_s; R = \frac{a}{\sinh \eta_s} \quad (2.6)$$

From eq 2.6, we determine

$$a = [(2R + s)s]^{1/2}, \cosh \eta_s = 1 + \frac{s}{R} \\ \eta_s = \ln \left\{ 1 + \frac{s}{R} + \left[\left(2 + \frac{s}{R} \right) \frac{s}{R} \right]^{1/2} \right\} \quad (2.7)$$

The electric potentials ψ_1 , ψ_2 , and ψ_3 , in the respective three dielectric phases, 1, 2, and 3, obey the Laplace equation

$$\nabla^2 \psi_1 = 0, \nabla^2 \psi_2 = 0, \nabla^2 \psi_3 = 0 \quad (2.8)$$

where ∇^2 denotes the Laplace operator. (The case in which phase 3 is an electrolyte solution is considered in section 3.2.) Because our system has rotational symmetry, the solution should not depend on the polar angle, φ . Therefore, the Laplace operator in bipolar coordinates is²³

$$\nabla^2 F = \frac{h^3}{a^2 \sin \xi} \left[\frac{\partial}{\partial \xi} \left(\frac{\sin \xi}{h} \frac{\partial F}{\partial \xi} \right) + \frac{\partial}{\partial \eta} \left(\frac{\sin \xi}{h} \frac{\partial F}{\partial \eta} \right) \right] \quad (2.9)$$

When ∇^2 is given by eq 2.9, it is known²⁴ that the variables in the equation, $\nabla^2 \psi = 0$, can be separated by introducing a new function, $F = h^{1/2} \tilde{F}$. Then, eq 2.9 acquires the form

$$\nabla^2 F = \frac{h^{5/2}}{a^2} \left[\frac{1}{\sin \xi} \frac{\partial}{\partial \xi} \left(\sin \xi \frac{\partial \tilde{F}}{\partial \xi} \right) + \frac{\partial^2 \tilde{F}}{\partial \eta^2} - \frac{\tilde{F}}{4} \right] \quad (2.10)$$

In such a case, the general solution of the Laplace equation can be presented as a series expansion:

(22) Arfken, G. *Mathematical Methods for Physicists*, 2nd ed.; Academic Press: London, 1970.

(23) Korn, G. A.; Korn, T. M. *Mathematical Handbook for Scientists and Engineers*, 2nd ed.; Dover: New York, 2000.

(24) Moon, P.; Spencer, D. E. *Field Theory Handbook, Including Coordinate Systems, Differential Equations, and Their Solutions*, 2nd ed.; Springer-Verlag: New York, 1988.

$$F = h^{1/2} \sum_{n=0}^{\infty} [X_n \exp(\lambda_n \eta) + Y_n \exp(-\lambda_n \eta)] P_n(\cos \xi), \lambda_n \equiv n + 1/2 \quad (2.11)$$

Here F stands for either of ψ_1 , ψ_2 , and ψ_3 ; P_n ($n = 0, 1, \dots$) are the Legendre polynomials;^{22,23} and X_n and Y_n are coefficients that have to be determined from the boundary conditions. In particular, the electric potential should be finite at the poles A_+ and A_- :

$$\psi_1 \rightarrow \text{const.}, \text{ at } \eta \rightarrow \infty \quad (2.12)$$

$$\psi_3 \rightarrow \text{const.}, \text{ at } \eta \rightarrow -\infty \quad (2.13)$$

The electric potentials should be equal at the phase boundaries 1–2 and 2–3:

$$\psi_1 = \psi_2 \text{ at } \eta = \eta_s \quad (2.14)$$

$$\psi_2 = \psi_3 \text{ at } \eta = 0 \quad (2.15)$$

With the help of the boundary conditions, eqs 2.12–2.15, from eq 2.11 we obtain

$$\psi_1 = \frac{Qh^{1/2}}{\epsilon_2 R} \sum_{n=0}^{\infty} [A_n \exp(2\lambda_n \eta_s) + B_n] \exp(-\lambda_n \eta) P_n(\cos \xi) \quad (2.16)$$

$$\psi_2 = \frac{Qh^{1/2}}{\epsilon_2 R} \sum_{n=0}^{\infty} [A_n \exp(\lambda_n \eta) + B_n \exp(-\lambda_n \eta)] P_n(\cos \xi) \quad (2.17)$$

$$\psi_3 = \frac{Qh^{1/2}}{\epsilon_2 R} \sum_{n=0}^{\infty} (A_n + B_n) \exp(\lambda_n \eta) P_n(\cos \xi) \quad (2.18)$$

in which A_n and B_n ($n = 0, 1, \dots$) are unknown dimensionless constants, which are to be determined from the boundary conditions for the normal electric-field components.

We assume that the surface charge density is zero at the planar boundary between phases 2 and 3, which leads to the following boundary condition:

$$\epsilon_2 \frac{\partial \psi_2}{\partial \eta} = \epsilon_3 \frac{\partial \psi_3}{\partial \eta} \text{ at } \eta = 0 \quad (2.19)$$

Substituting eqs 2.17 and 2.18 into eq 2.19, we obtain a relation between the constants A_n and B_n :

$$B_n = \beta_{23} A_n \quad (n = 0, 1, \dots) \quad (2.20)$$

in which we have introduced the notation

$$\beta_{ij} \equiv \frac{\epsilon_i - \epsilon_j}{\epsilon_i + \epsilon_j} \quad (i, j = 1, 2, 3) \quad (2.21)$$

Note that $-1 < \beta_{ij} < 1$. Especially, we have $\beta_{23} \rightarrow -1$ for $\epsilon_3 \gg \epsilon_2$ (e.g., phase 3 is water and phase 2 is oil). For $\beta_{23} = -1$, eq 2.20 yields $B_n = -A_n$, and eq 2.18 reduces to $\psi_3 = 0$; that is, the electric potential is zero at the planar interface ($z = 0$) and inside phase 3.

The boundary condition for the normal electric-field components at the particle surface is

$$\mathbf{e}_\eta \cdot (\epsilon_1 \nabla \psi_1 - \epsilon_2 \nabla \psi_2) = -4\pi\sigma \text{ at } \eta = \eta_s \quad (2.22)$$

In view of eq 2.4, eq 2.22 acquires the form

$$\epsilon_1 \frac{\partial \psi_1}{\partial \eta} - \epsilon_2 \frac{\partial \psi_2}{\partial \eta} = -4\pi\sigma \frac{a}{h} \text{ at } \eta = \eta_s \quad (2.23)$$

Further, we substitute eqs 2.16 and 2.17 into eq 2.23 and take into account eq 2.20; thus, we determine the constants A_n ($n = 0, 1, \dots$) (see section 4.1 below).

2.2. Electrostatic Force and Energy. In accordance with Newton's third law, the electrostatic force acting on the particle, F_z , is opposite to the force acting on the flat interface, S_{23} , between phases 2 and 3. The same conclusion follows from the field theory:²⁰ The divergence of the Maxwell stress tensor is zero in phase 2. Then, in accordance with the Gauss theorem, one obtains that the sum of the integrals over S_{12} and S_{23} must be zero; that is, these two integrals are equal (by magnitude) with the opposite signs. Therefore, we can calculate F_z by integrating the Maxwell stress over the surface S_{23} that coincides with the xy -plane:

$$F_z = -\frac{\epsilon_2}{8\pi} \int_{S_{23}} \left[\left(\frac{\partial \psi_2}{\partial z} \right)^2 - \left(\frac{\partial \psi_2}{\partial x} \right)^2 - \left(\frac{\partial \psi_2}{\partial y} \right)^2 \right] dS_{23} \text{ at } z = 0 \quad (2.24)$$

In view of eq 2.20, by substitution of eq 2.17 in eq 2.24 and integration, one can derive an exact formula for the force acting on the particle (see Appendix B in the Supporting Information):

$$F_z = \frac{\beta_{23} Q^2}{4\epsilon_2 (R + s)^2} f_z \quad (2.25)$$

Here $F_z > 0$ means that the phase boundary 2–3 repels the particle, whereas $F_z < 0$ corresponds to attraction; the dimensionless force coefficient, f_z , is

$$f_z = \left(1 + \frac{s}{R} \right)^2 \sum_{n=0}^{\infty} [(4n + 2)A_n^2 - (4n + 4)A_n A_{n+1}] \quad (2.26)$$

The coefficients A_n can be calculated numerically, as described in section 4. It is important to note that f_z depends only on the dimensionless distance, s/R , and on the parameters β_{12} and β_{23} defined by eq 2.21.

In view of eq 2.25, the electrostatic energy of interaction between the particle and phase 3 is

$$W = \int_s^{\infty} F_z ds = \frac{\beta_{23} Q^2}{4\epsilon_2 (R + s)} w \quad (2.27)$$

where the definition of the dimensionless energy coefficient, w , is

$$w \equiv \left(1 + \frac{s}{R} \right) \int_{s/R}^{\infty} \frac{f_z}{(1 + \tilde{s})^2} d\tilde{s} \quad (\tilde{s} \equiv s/R) \quad (2.28)$$

In the special case where $\epsilon_1 = \epsilon_2$, the above equations considerably simplify (see section 3.1). Numerical results for f_z and w at various s/R , β_{12} , and β_{23} are presented and discussed in section 5.

3. The Special Case $\epsilon_1 = \epsilon_2$

3.1. Phase 3 is a Common Dielectric. In the special case where $\epsilon_1 = \epsilon_2$, one can determine the electric potential $\psi(\mathbf{r})$ by means of the method of reflections.^{20,25} (The alternative approach of Legendre-polynomial expansion, eq 2.11, gives the same result;

see the comment after eq 4.5.) Following an approach analogous to that used in ref 20, one can obtain the electric potential in phase 2 as a superposition of electric potentials induced by two charges located at the axis of revolution. The first is situated at $z = R + s$ (at the particle center), whereas the second one is placed at $z = -(R + s)$; that is, it is the mirror image of the former charge with respect to the plane $z = 0$:

$$\psi_2 = \frac{Q}{\epsilon_2} \left\{ \frac{1}{[r^2 + (z - R - s)^2]^{1/2}} + \frac{\beta_{23}}{[r^2 + (z + R + s)^2]^{1/2}} \right\} \quad (3.1)$$

The electric potential in phase 1 (inside the particle) is obtained as a superposition of a constant potential, $Q/(\epsilon_2 R)$, and the potential induced by the image charge at $z = -(R + s)$:

$$\psi_1 = \frac{Q}{\epsilon_2} \left\{ \frac{1}{R} + \frac{\beta_{23}}{[r^2 + (z + R + s)^2]^{1/2}} \right\} \quad (3.2)$$

The electric potential in phase 3 is induced only by the original charge at $z = R + s$:

$$\psi_3 = \frac{Q}{\epsilon_2} \frac{1 + \beta_{23}}{[r^2 + (z - R - s)^2]^{1/2}} \quad (3.3)$$

The substitution of eq 3.1 into eq 2.24, after some transformations, gives the interaction force in the form of 2.25 with $f_z = 1$:

$$F_z = \frac{\beta_{23} Q^2}{\epsilon_2 [2(R + s)]^2} \quad (3.4)$$

As in the case of point charge,²⁰ eq 3.4 expresses the force of interaction between the original charge, Q , and the image charge, $-\beta_{23}Q$, which are separated at a distance $2(R + s)$. In other words, the physical origin of the particle–interface interaction, considered in the present article, is the image-force effect. Because we are dealing with a particle of finite size (rather than with a point ion), the force given by eq 3.4 has a finite value at contact (at $s = 0$). The substitution of eq 3.4 into eq 2.28 leads to eq 2.27 with $w = 1$:

$$W = \frac{\beta_{23} Q^2}{4\epsilon_2 (R + s)} \quad (3.5)$$

As it could be expected, the interaction energy also has a finite value at contact (at $s = 0$). The additional multipliers f_z and w in eqs 2.25 and 2.27 (in comparison with eqs 3.4 and 3.5) account for the fact that, in general, the particle may have a different dielectric constant from the surrounding medium; that is, $\epsilon_1 \neq \epsilon_2$.

It has been proven (see ref 26, p 408) that the method of reflections cannot be applied when $\epsilon_1 \neq \epsilon_2$. Therefore, in the latter case, it is impossible to obtain simple analytical expressions like eqs 3.4 and 3.5. Instead, one has to use the series, eq 2.26, which enables one to calculate exactly the interaction force and energy, F_z and W , for $\epsilon_1 \neq \epsilon_2$ (see sections 4 and 5).

3.2. Phase 3 is Water. Here, we consider the important special case when phase 3 is water. Water always contains dissolved ions. Even the ideal pure water has an ionic strength of 10^{-7} M due to the inevitable H^+ and OH^- ions. The presence of ions

(25) Happel, J.; Brenner, H. *Low Reynolds Number Hydrodynamics*; Prentice Hall: New York, 1965.

(26) Grinberg, G. A. *Selected Problems of the Mathematical Theory of Electric and Magnetic Phenomena*; Publishing House of the Academy of Sciences of USSR: Moscow, 1948 (in Russian).

implies that the Laplace equation, $\nabla^2\psi_3 = 0$, must be replaced by the Poisson equation, $\nabla^2\psi_3 = -(4\pi/\epsilon_3)\rho$, in which ρ is the bulk charge density. In principle, this could affect the force and energy coefficients, f_z and w , in eqs 2.25 and 2.27.

It is important to note that water has a high dielectric constant, $\epsilon_3 \gg \epsilon_2$. In view of eq 2.21, this means that β_{23} is close to -1 . As discussed after eq 2.21, $\beta_{23} = -1$ implies that $B_n = -A_n$, and therefore $\psi_3 = 0$ (see eq 2.18). In other words, the electric field, created by the charged particle into the oil (phase 2), does not enter the water (phase 3). Actually, some weak electric field could enter the water phase because β_{23} is slightly different from -1 (for tetradecane–water at 25 °C, we have $\epsilon_2 = 2.04$, $\epsilon_3 = 78.2$, and then $\beta_{23} = -0.95$).

Thus, it turns out that the high dielectric constant of water suppresses the penetration of the particle electric field into the aqueous phase. If the latter contains dissolved ions, the penetration of the particle-induced electric field will be additionally suppressed because of the Debye screening effect.²⁷ Hence, we could expect that, if phase 3 is water, then eq 3.4 could be expressed in the form

$$F_z = \frac{B_{23}Q^2}{\epsilon_2[2(R+s)]^2} \quad (3.6)$$

where

$$-1 \leq B_{23} \leq \beta_{23} \approx -0.95 \quad (3.7)$$

In eq 3.7, the lower limit, $B_{23} = -1$, corresponds to high electrolyte concentrations in the water ($2\kappa(R+s) \gg 1$; see Appendix A) when the aqueous phase becomes conductor of electricity (for conductors, $\epsilon_3 \rightarrow \infty$). The upper limit, $B_{23} = \beta_{23} \approx -0.95$, corresponds to the case of negligibly small ionic strength (deionized water, $\epsilon_3 \approx 80$). Hence, the addition of electrolyte in the aqueous phase leads to a variation of B_{23} in the frame of only 5%. In Appendix A, we have derived eq 3.7 for the simpler case in which $\epsilon_1 = \epsilon_2$ and for when the electric potential into water is low so that the Poisson–Boltzmann equation can be linearized.²⁷ The general case of nonlinear electric-double-layer theory and $\epsilon_1 \neq \epsilon_2$ demands the application of more complicated mathematics and a numerical solution, but the result is unlikely to differ from eq 3.7, insofar as $\epsilon_3 \gg \epsilon_1, \epsilon_2$.

In summary, the effect of electrolyte in phase 3 (water) on F_z and W turns out to be relatively weak, in the frame of 5% (see eq 3.7). In the following, we will set $\beta_{23} = -1$ when phase 3 is an aqueous electrolyte solution, and $\beta_{23} = -0.95$ for the deionized water/oil boundary. Of course, B_{23} is expected to vary from -0.95 to -1 with the increase of electrolyte concentration (see eqs A.16 and A.17 in Appendix A). However, the general theoretical description of this variation is mathematically complicated and could be the subject of a separate study.

4. Determination of the Coefficients A_n

4.1. System of Equations for A_n . Here, we return to the general case in which $\epsilon_1 \neq \epsilon_2 \neq \epsilon_3$, considered in section 2. After a substitution of eqs 2.16 and 2.17 into the boundary condition, eq 2.23, and after elimination of the constants B_n by using eq 2.20, one can derive (Appendix C in the Supporting Information)

$$\sum_{n=0}^{\infty} [2(\cosh \eta_s - u)(1 + \beta_{12}C_n)\lambda_n - \beta_{12} \sinh \eta_s(1 + C_n)]D_n = \frac{(1 - \beta_{12}) \sinh \eta_s}{(\cosh \eta_s - u)^{1/2}} \quad (4.1)$$

in which $C_n = \beta_{23} \exp(-2\lambda_n\eta_s)$, $D_n = A_n \exp(\lambda_n\eta_s)P_n(u)$, $u = \cos \xi$, and $\lambda_n = n + 1/2$. Because the Legendre polynomials, $P_n(u)$, are orthogonal over the interval $[-1, 1]$, from eq 4.1 we obtain a three-diagonal linear system of equations for the coefficients A_n , $n = 0, 1, \dots$ (Appendix C in the Supporting Information):

$$[1 - \beta_{12} + (1 + \beta_{12})t^2 + 2\beta_{12}\beta_{23}t^3]A_0 - 2(1 + \beta_{12}\beta_{23}t^3)A_1 = 2^{1/2}(1 - \beta_{12})(t - t^3) \quad (4.2)$$

$$- 2nt^2(1 + \beta_{12}\beta_{23}t^{2n-1})A_{n-1} + \{2(1 + t^2)\lambda_n - (1 - t^2)\beta_{12} + [2(1 + t^2)\lambda_n - (1 - t^2)]\beta_{12}\beta_{23}t^{2n+1}\}A_n - 2(n+1)(1 + \beta_{12}\beta_{23}t^{2n+3})A_{n+1} = 2^{1/2}(1 - \beta_{12})(1 - t^2)t^{2n+1} \quad (n \geq 1) \quad (4.3)$$

in which $t \equiv \exp(-\eta_s)$. It is important to note that the asymptotic form of eq 4.3 for $n \gg 1$ is

$$- 2nt^2A_{n-1} + [(2n+1)(1 + t^2) - \beta_{12}(1 - t^2)]A_n - 2(n+1)A_{n+1} \approx 2^{1/2}(1 - \beta_{12})(1 - t^2)t^{2n+1} \quad (n \gg 1) \quad (4.4)$$

The system defined by eq 4.4 has a simple solution:

$$A_n = 2^{1/2}t^{2n+1} \quad (n \gg 1) \quad (4.5)$$

In addition, one could check that, in the case of equal dielectric constants of phases 1 and 2, that is, $\beta_{12} = 0$, the solution of system 4.2–4.3 is given by eq 4.5 for all n . Then, the series in eq 2.26 can be summed exactly and gives $f_z = 1$; correspondingly, $w = 1$ in eq 2.28. This results shows that eqs 3.4 and 3.5, derived by means of the reflection method for $\epsilon_1 = \epsilon_2$, also represent the special cases of eqs 2.25–2.28, which are based on series expansions in terms of Legendre polynomials.

4.2. Principles of the Computational Procedure. The numerical algorithm for solution of the system of eqs 4.2–4.3 is the following: For a given s/R , we determine η_s (and $t = \exp(-\eta_s)$) from eq 2.7. Next, we choose a sufficiently large number, N , for which we have $t^{2N+1} < \delta$, where δ determines the precision of the numerical calculations. For $n \geq N$, we calculate the coefficients A_n from the asymptotic expression, eq 4.5. For $0 \leq n \leq N-1$, we determine A_n by solving exactly the three-diagonal system of eqs 4.2–4.3 by using the Thomas algorithm.²⁸ Following this numerical scheme, the solution of the system for the coefficients A_n could be found with very high accuracy. Next, the force is calculated from eqs 2.25 and 2.26. Finally, the interaction energy is determined from eqs 2.27 and 2.28 by numerical integration.

5. Numerical Results and Discussion

5.1. Interaction Energy for Typical Parameter Values. Let us consider the following example: glass particle in tetradecane near the tetradecane–water boundary. For this system, the surface charge density at the particle–oil interface was experimentally determined¹⁶ to be $\sigma = 71 \mu\text{C}/\text{m}^2$. We have $\epsilon_1 = 3.97$, $\epsilon_2 = 2.04$,

(27) Overbeek, J. Th. G. *Electrochemistry of the double layer*, In *Colloid Science*; Kruyt, H. R., Ed.; Elsevier: Amsterdam, 1953; Vol. 1.

(28) Press, W. H.; Teukolsky, S. A.; Vetterling, W. T.; Flannery, B. P. *Numerical Recipes in Fortran. The Art of Scientific Computing*, 2nd ed.; Cambridge University Press: Cambridge, U.K., 1992.

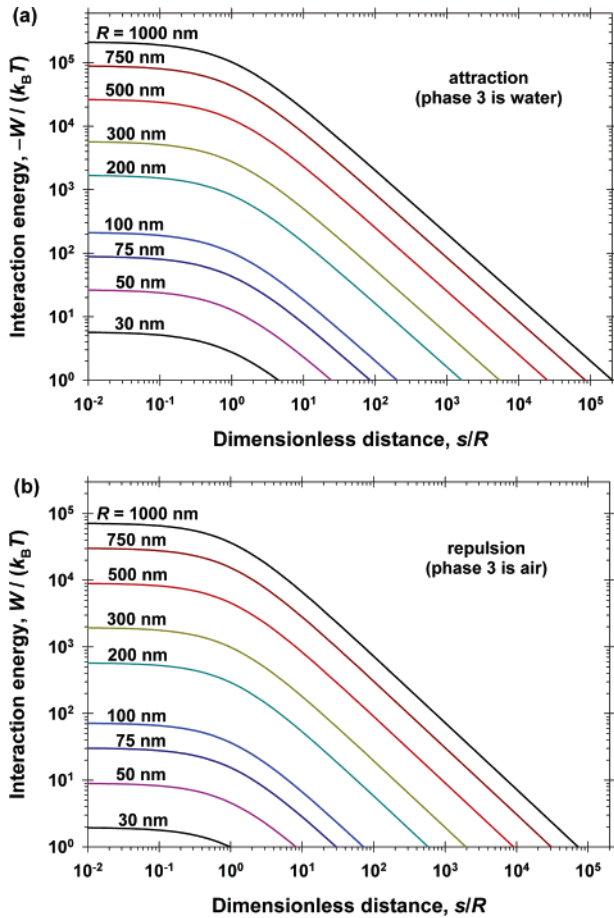


Figure 4. Plot of the interaction energy W (scaled with $k_B T$) vs the dimensionless distance, s/R , between a charged glass particle and a planar interface; phase 2 is tetradecane. The curves correspond to different particle radii, R , denoted in the figure; the other parameter values are given in the text. (a) Phase 3 is water. (b) Phase 3 is air.

and $\epsilon_3 = 78.2$, respectively, for the glass, tetradecane, and water, at 25 °C. Then, $\beta_{12} = 0.32$. When phase 3 is water or air, we have, respectively, $\beta_{23} = -0.95$ and $\beta_{23} = +0.34$. In accordance with eq 2.27, $\beta_{23} < 0$ corresponds to attraction, whereas $\beta_{23} > 0$ corresponds to repulsion between the particle and the oil–water interface.

In Figure 4, numerical results for the interaction energy, W , scaled by the thermal energy $k_B T$, are plotted versus the relative distance, s/R , for various values of the particle radius, R ; the other parameter values have been specified above. In general, the curves in Figure 4 correspond to a strong and long-range particle–interface interaction, which is *attraction* if phase 3 is water (Figure 4a), but is *repulsion* if phase 3 is air (Figure 4b). For the given surface charge density ($\sigma = 71 \mu\text{C}/\text{m}^2$), the interaction energy, W , becomes comparable to or smaller than the thermal energy $k_B T$ for $R < 30$ nm. On the other hand, for $R > 30$ nm, W strongly increases with the particle size and reaches $W \approx 10^5 k_B T$ for $R = 1 \mu\text{m}$ at close contact. In addition, the range of the interaction also strongly increases, reaching $s/R \approx 10^5$ for $R = 1 \mu\text{m}$. The strong effect of the particle radius follows from eq 2.27, which could be expressed in the form

$$W = \frac{4\pi^2 \sigma^2 R^3 \beta_{23}}{\epsilon_2 (1 + s/R)} w(s/R, \beta_{12}, \beta_{23}) \quad (5.1)$$

Here, $w(s/R, \beta_{12}, \beta_{23})$ is a function of bounded variation (see below), so the major effect of the particle radius on the interaction

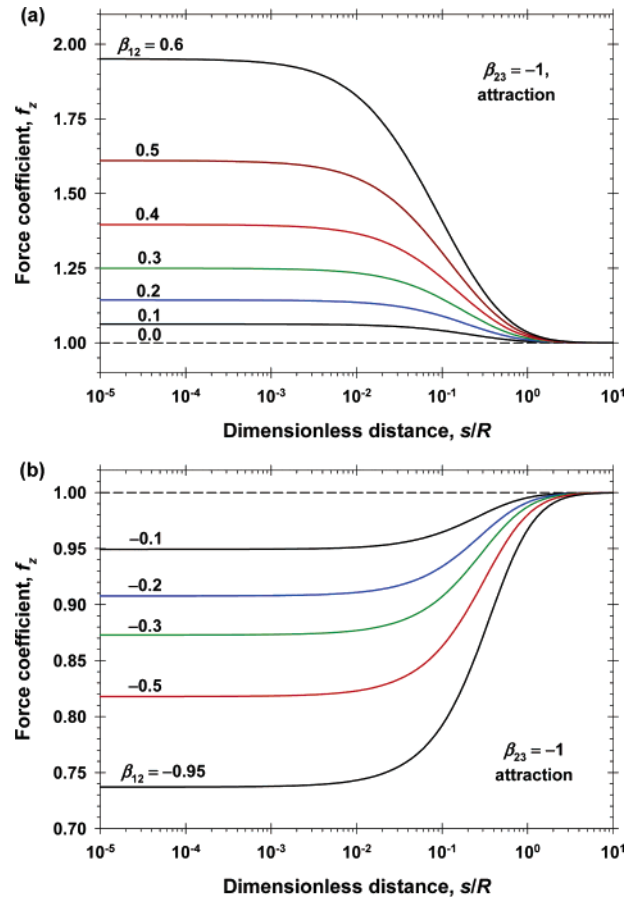


Figure 5. The force coefficient, f_z , as a function of the dimensionless distance, s/R , for fixed $\beta_{23} = -1$ (i.e., $\epsilon_3 \gg \epsilon_2$, which is satisfied for the oil–water interface), and for various β_{12} denoted in the figure.

energy is due to the multiplier $R^3/(1 + s/R)$ in eq 5.1. The fact that the bilogarithmic plots of W versus s/R in Figure 4 are parallel lines for large s/R is due to the asymptotic form of eq 5.1:

$$W \approx \frac{4\pi^2 \sigma^2 R^4 \beta_{23}}{\epsilon_2 s} \quad \text{for } s/R \gg 1 \quad (5.2)$$

Here, we have used the fact that $w \approx 1$ for $s/R > 1$ (see the subsequent figures).

In summary, we are dealing with a significant effect, which can force particles initially dispersed in the oily phase to adsorb at the oil–water interface (see Figures 1b and 4a). This result is of central importance for the production of particle-stabilized emulsions. The rest of this section is focused on the behavior of the functions $w(s/R, \beta_{12}, \beta_{23})$ and $f_z(s/R, \beta_{12}, \beta_{23})$.

5.2. Effect of β_{12} in the Case Where $\beta_{23} \approx -1$ (e.g., Aqueous Phase 3). As discussed above, when phase 3 is an aqueous electrolyte solution (or whatever phase of high dielectric constant), then β_{23} is close to -1 . In this case, eqs 2.25 and 5.1 predict *attraction* between the particle and interface. Numerical results for the force coefficient, f_z , calculated as explained in section 4.2, are shown in Figure 5. If $\epsilon_1 > \epsilon_2$, then $\beta_{12} > 0$, and we obtain $f_z > 1$ (Figure 5a). In the opposite case, $\epsilon_1 < \epsilon_2$ and $\beta_{12} < 0$, we obtain $f_z < 1$ (Figure 5b). If we compare the curves for f_z in panels a and b of Figure 5, we see that the relative influence of β_{12} on f_z is greater in the case where $\beta_{12} > 0$. The dashed line, $f_z = 1$, corresponds to equal dielectric constants; that is, $\epsilon_1 = \epsilon_2$ and $\beta_{12} = 0$ (see eq 3.4).

The numerical results for the energy coefficient w (see eq 2.28) are shown in Figure 6. The curves in Figures 5 and 6 look

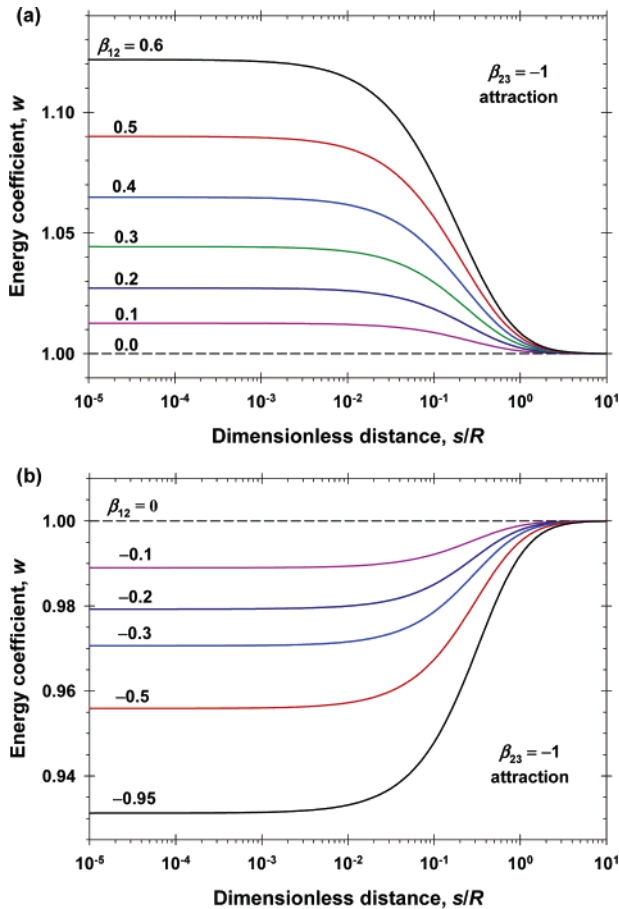


Figure 6. The energy coefficient, w , as a function of the dimensionless distance, s/R , for fixed $\beta_{23} = -1$ (i.e. $\epsilon_3 \gg \epsilon_2$, which is satisfied for the oil–water interface), and for various β_{12} denoted in the figure.

similar, but the values on the ordinate axes indicate that the variation of β_{12} produces a weaker effect on w in comparison with f_z . On the other hand, the general trend of f_z and w is similar: both of them increase with the increase in β_{12} , and both of them tend to 1 for $s/R > 1$.

The deviation of f_z and w from 1 is the greatest at contact, that is, at $s = 0$. We have $f_z \approx f_z(0)$ and $w \approx w(0)$ for $s/R < 10^{-2}$ (see Figures 5 and 6). The dependencies of $f_z(0)$ and $w(0)$ on β_{12} , for $\beta_{23} = -1$, are given in Figure 7. These dependencies are accurately interpolated by means of the following expressions:

$$f_z(0) = (1 - \beta_{12})^{-3/2} (1 - 0.9386\beta_{12} + 0.1410\beta_{12}^2 + 0.0226\beta_{12}^3 + 0.0111\beta_{12}^4) \quad (5.3)$$

$$w(0) = (1 - \beta_{12})^{-3/2} (1 - 1.3833\beta_{12} + 0.2760\beta_{12}^2 + 0.0541\beta_{12}^3 + 0.0272\beta_{12}^4) \quad (5.4)$$

For $-0.95 \leq \beta_{12} \leq +0.95$, the accuracy of eqs 5.3 and 5.4 is better than 1% and 0.1%, respectively.

For a more convenient computation of the dependencies of $f_z(s/R, \beta_{12})$ and $w(s/R, \beta_{12})$ (see the curves in Figures 5 and 6), we obtained accurate interpolation formulas, as follows:

$$f_z(\eta_s) = 1 + [f_z(0) - 1] \exp\{a_1[1 - \exp(-b_1\eta_s)] + a_2[1 - \exp(-b_2\eta_s)] - 3\eta_s\} \quad (5.5)$$

$$w(\eta_s) = 1 + [w(0) - 1] \exp\{a_3[1 - \exp(-b_3\eta_s)] - 3\eta_s\} \quad (5.6)$$

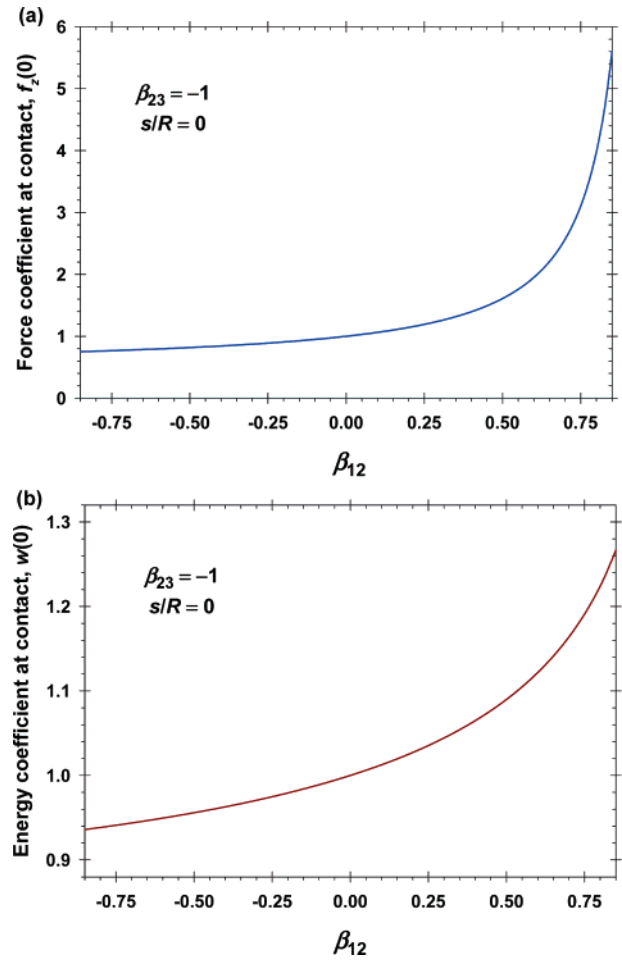


Figure 7. (a) Force coefficient, $f_z(0)$, and (b) energy coefficient, $w(0)$, plotted vs β_{12} for fixed $\beta_{23} = -1$ and $s/R = 0$. The latter value corresponds to a point contact of the spherical particle with the planar interface.

Table 1. The Coefficients in Eqs 5.5 and 5.6 for Various β_{12}

β_{12}	a_1	b_1	a_2	b_2	a_3	b_3
-0.95	2.1369	1.6601	0	0	2.0006	1.7449
-0.5	1.8537	1.8780	0	0	1.8990	1.7392
-0.3	1.7566	1.9374	0	0	1.8521	1.7724
-0.2	1.6997	1.9740	0	0	1.8259	1.7943
-0.1	1.6354	2.0167	0	0	1.7968	1.8185
0.1	1.4780	2.1270	0	0	1.7252	1.8692
0.2	1.2296	2.3361	0.15393	1.2836	1.6808	1.8895
0.3	0.37249	3.7971	0.89831	1.8364	1.6275	1.9051
0.4	0.31101	5.1660	0.82345	1.7796	1.5635	1.9120
0.5	0.29731	6.6758	0.66725	1.6470	1.4863	1.9075
0.6	0.26771	9.1370	0.47725	1.4123	1.3938	1.8946

where the coefficients $f_z(0)$ and $w(0)$ have to be calculated from eqs 5.3 and 5.4, and η_s is given by eq 2.7. The coefficients a_1 , b_1 , a_2 , b_2 , a_3 , and b_3 are listed in Table 1 for various β_{12} . For $-0.95 \leq \beta_{12} \leq +0.6$, the accuracy of eqs 5.5 and 5.6 is better than 1% and 0.1%, respectively. For values of β_{12} that are intermediate between those given in Table 1, the values of the coefficients a_i and b_i ($i = 1, 2, 3$) could be determined by interpolation.

At short distances ($s \rightarrow 0$), eq 2.7 gives $\eta_s \rightarrow 0$, and then eqs 5.5 and 5.6 reduce to $f_z = f_z(0)$ and $w = w(0)$, as could be expected. In the other limit, $s \rightarrow \infty$, we have $\eta_s \rightarrow \infty$, and then eqs 5.5 and 5.6 give the correct asymptotics at long distances, viz. $f_z = w = 1$ (see Figures 5 and 6).

5.3. Effect of β_{23} on the Force and Energy Coefficients, w and f_z . In general, eqs 2.25 and 2.27 predict that, if $\epsilon_2 < \epsilon_3$ and

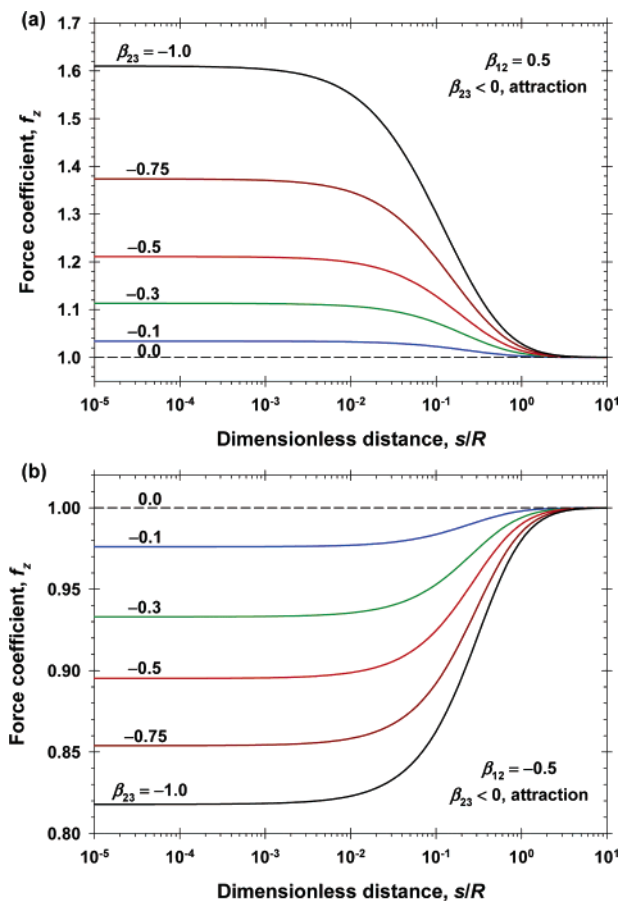


Figure 8. Plot of the force coefficient, f_z , vs the dimensionless distance, s/R , for various negative values of β_{23} denoted in the figure. (a) $\beta_{12} = 0.5$. (b) $\beta_{12} = -0.5$.

$\beta_{23} < 0$, the interaction force is *attractive*, whereas, if $\epsilon_2 > \epsilon_3$ and $\beta_{23} > 0$, the force corresponds to *repulsion*. Our aim here is to present numerical results for the force and energy coefficients, f_z and w , which have been obtained by means of the exact computational procedure in section 4.2. The values of $f_z(s/R, \beta_{12}, \beta_{23})$ and $w(s/R, \beta_{12}, \beta_{23})$ are necessary for the exact calculation of the interaction force and energy.

Figure 8 presents numerical data for f_z versus s/R in the case where $\beta_{23} < 0$ (attraction). In addition, Figure 9 shows numerical data for f_z versus s/R in the case where $\beta_{23} > 0$ (repulsion). The respective curves for $w(s/R)$ look similar to those for $f_z(s/R)$, but correspond to somewhat different absolute values. To illustrate the effect of β_{12} , we compare the curves calculated for $\beta_{12} = 0.5$ (Figures 8a and 9a) with the respective curves calculated for $\beta_{12} = -0.5$ (Figures 8b and 9b).

In the case where $\beta_{12} = 0.5$, f_z decreases when β_{23} increases (Figures 8a and 9a). In contrast, for $\beta_{12} = -0.5$, f_z increase when β_{23} increases (Figures 8b and 9b). In all cases, f_z levels off at 1 for $s/R > 1$. On the other hand, for $s/R < 0.01$, f_z takes a finite value, $f_z(0)$, corresponding to contact of the particle with the oil–water interface.

In Figure 10, the calculated values of $f_z(0)$ and $w(0)$ are plotted versus β_{23} for various β_{12} . This figure visualizes the effect of β_{12} and β_{23} on the *magnitude* of the force and energy coefficients. Note that $f_z(0) = 1$ and $w(0) = 1$ correspond to the conventional image force, that is, the force experienced by a *point* charge (rather than a particle of finite size) near the boundary between two dielectric phases. In Figure 10, this is the case for $\beta_{12} = 0$ (the dashed horizontal line), which corresponds to a particle having the same dielectric constant as the surrounding fluid (e.g.,

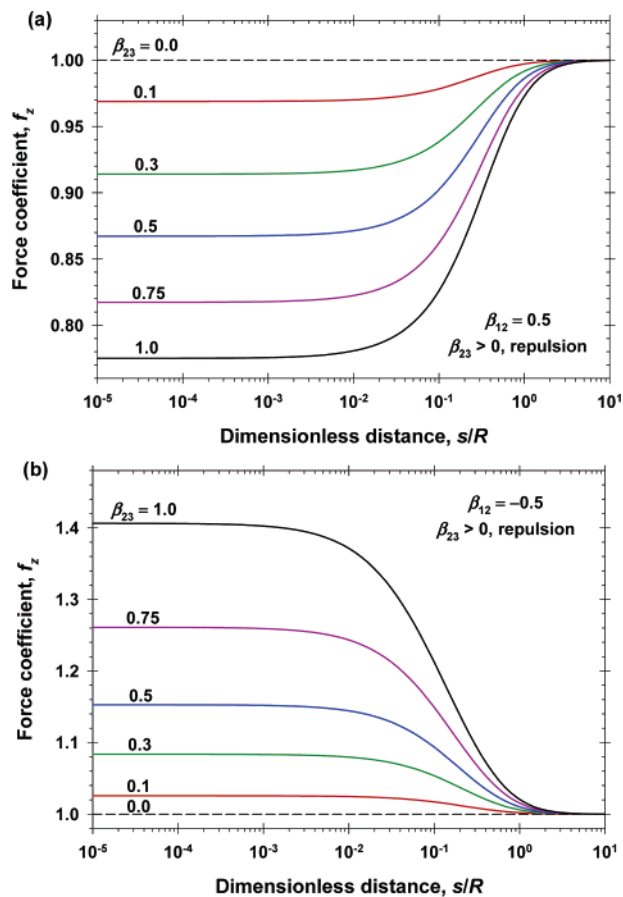


Figure 9. Plot of the force coefficient, f_z , vs the dimensionless distance, s/R , for various positive values of β_{23} denoted in the figure. (a) $\beta_{12} = 0.5$. (b) $\beta_{12} = -0.5$.

oil; see section 3.1). For $\beta_{23} = 0$, we again have $f_z(0) = w(0) = 1$; however, in this case, the force and energy, F_z and W , are equal to zero because of the multiplier β_{23} in eqs 2.25 and 2.27. Indeed, from a physical viewpoint, in the latter case, there is no particle–interface interaction because, at $\epsilon_2 = \epsilon_3$, the electric field does not feel the presence of a boundary between phases 2 and 3. Figure 10 also shows that the greatest deviations from the conventional image force (from $f_z(0) = w(0) = 1$) occur at the greatest absolute values of β_{12} and β_{23} .

It should be noted that the effect of β_{23} on the force, F_z , and energy, W , is much stronger than its effect on the force and energy coefficients, f_z and w , because β_{23} appears explicitly as a multiplier in eqs 2.25 and 2.27. In addition, as demonstrated in section 3.2 and Appendix A, the presence of electrolyte in the aqueous phase does not alter the overall picture: it turns out that the case in which phase 3 is water and phase 2 is a nonpolar liquid can be described by the above results for f_z and w with $\beta_{23} \approx -1$ (see Figures 5–7 and eqs 5.5 and 5.6).

It should be noted also that here we have considered the case in which the particle approaches the flat interface at fixed *surface charge density*, σ . In the case of hydrophobic dielectric particles in oil, possible hypotheses about the origin of σ have been discussed in refs 18 and 19. The alternative case of fixed *particle surface potential* is not considered here; it could be the subject of a separate study. Note that, at fixed surface electric potential, the particle–interface interaction becomes independent of the particle dielectric constant, ϵ_1 . Consequently, the case of fixed surface potential is physically rather different from the case of fixed surface charge considered here.

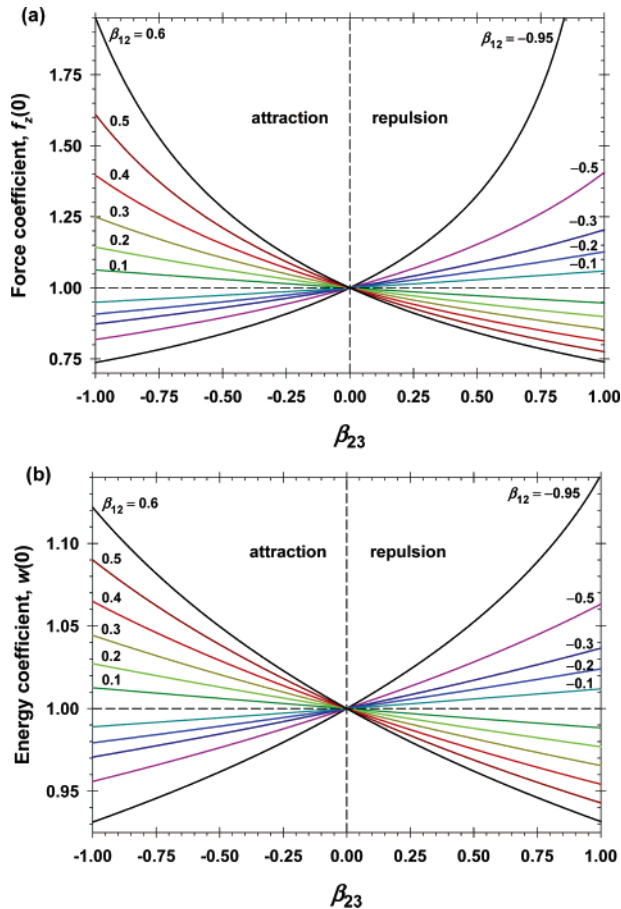


Figure 10. Force and energy coefficients, $f_z(0)$ and $w(0)$, at the contact of the spherical particle with the planar interface ($s/R = 0$), plotted vs β_{23} for various β_{12} .

6. Summary and Conclusions

Quantitative theory of the particle–interface interaction across a nonpolar medium is developed. We consider a spherical dielectric particle (phase 1), which is immersed in a nonpolar medium (phase 2), near its boundary with a third dielectric medium (phase 3) (see Figure 2). This interaction originates from electric charges at the interface particle/nonpolar phase (e.g., particle/oil). The theoretical problem is solved exactly, in terms of Legendre polynomials, for arbitrary values of the dielectric constants of the three phases. As a result, expressions for calculating the interaction force and energy, eqs 2.25 and 2.27, are derived. These expressions generalize the known theory of the electrostatic image force (acting on point charges) to the case of particles that have finite size, uniform surface charge density, and specific dielectric constant, ϵ_1 . The deviation from the conventional image-force interaction is considerable at particle-to-interface distances smaller than the particle radius ($f_z \neq 1$ and $w \neq 1$ for $s/R < 1$; see Figures 5, 6, and 8–10).

For typical parameter values (glass or silica particle immersed in liquid paraffin), the image-force interaction becomes significant for particles of radius $R > 30$ nm (see Figure 4). Of course, if the surface charge density is greater, the effect will become significant for smaller particles. For a fixed relative particle-to-interface distance (s/R), the respective force and energy increase with the cube of the particle radius. In general, this is a strong and long-range interaction. For example, for micrometer-sized particles, the interaction energy could be on the order of $10^5 k_B T$ at close contact, whereas the interaction range is about 10^5 particle radii (Figure 4).

As usual for image forces, the sign of the particle–interface interaction depends on the difference between the dielectric constants of phases 2 and 3. When phase 3 has a smaller dielectric constant (e.g., when phase 3 is air), the interface repels the particle (Figure 4b). In contrast, when phase 3 has a greater dielectric constant (e.g., when phase 3 is water), the interaction is attractive (Figure 4a). Thus, water drops attract charged hydrophobic particles dispersed in the oily phase, and, in this way, favor the formation of reverse particle-stabilized (Pickering) emulsions (Figure 1b). This could be one of the reasons for the easier production of reverse Pickering emulsions in comparison with the production of direct ones. It should also be noted that the particle–interface interaction across the oily phase is insensitive to the concentration of electrolyte in the aqueous phase 3 (see sections 3.2 and Appendix A).

Acknowledgment. We gratefully acknowledge the support of Unilever Research & Development, Trumbull, Connecticut, for this study.

Appendix A: Effect of Electrolyte in Phase 3 on the Particle–Interface Interaction

To derive eq 3.7, we will consider the simpler case where $\epsilon_1 = \epsilon_2$ and where the electric potential into water (phase 3) is low so that the Poisson–Boltzmann equation can be linearized:²⁷

$$\nabla^2 \psi_3 = \kappa^2 \psi_3, \quad \kappa^2 = \frac{4\pi e^2}{\epsilon_3 k_B T} \sum_i Z_i^2 c_i \quad (\text{A.1})$$

Here, κ is the Debye screening parameter, e is the elementary electric charge, c_i and Z_i are the concentrations of the ionic species and their valences, and the summation is carried out over all ionic species in the water phase. In general, ψ_3 can be expressed in the form

$$\psi_3 = \psi_0 + \tilde{\psi}_3 \quad (\text{A.2})$$

in which ψ_0 is the electric potential in the aqueous phase in the absence of the particle (phase 1 in Figure 2), while $\tilde{\psi}_3$ is the electric field induced by this particle into the aqueous phase. Correspondingly, ψ_0 and $\tilde{\psi}_3$ obey eq A.1 and the following boundary conditions at the interface between phases 2 and 3:

$$\epsilon_3 \frac{\partial \psi_0}{\partial z} = 4\pi \sigma_{23} \quad \text{and} \quad \epsilon_3 \frac{\partial \tilde{\psi}_3}{\partial z} = \epsilon_2 \frac{\partial \psi_2}{\partial z} \quad \text{at } z = 0 \quad (\text{A.3})$$

Here, σ_{23} is the surface electric charge density at the boundary 2–3. Thus, for $\psi_0(z)$, we will obtain the conventional expression for the electric potential of a planar electric double layer of surface charge σ_{23} .²⁷ On the other hand, $\tilde{\psi}_3$ is independent of σ_{23} . In addition, we will seek ψ_2 and ψ_1 in the form

$$\psi_2 = \frac{Q}{\epsilon_2} \frac{1}{[r^2 + (z-b)^2]^{1/2}} + \tilde{\psi}_2 \quad (\text{A.4})$$

$$\psi_1 = \frac{Q}{\epsilon_2} \frac{1}{R} + \tilde{\psi}_2 \quad (\text{A.5})$$

where $b \equiv R + s$, and $\tilde{\psi}_2$ obeys the Laplace equation, $\nabla^2 \tilde{\psi}_2 = 0$. In addition, we have $\nabla^2 \tilde{\psi}_3 = \kappa^2 \tilde{\psi}_3$. To satisfy the latter equations, in view of the geometry of the system, we will seek $\tilde{\psi}_2$ and $\tilde{\psi}_3$ in the form of Hankel transforms:

$$\tilde{\psi}_2 = \int_0^\infty C_2 e^{-kz} J_0(kr) k dk \quad (\text{A.6})$$

$$\tilde{\psi}_3 = \int_0^\infty C_3 e^{qz} J_0(kr) k dk, \quad q \equiv (k^2 + \kappa^2)^{1/2} \quad (\text{A.7})$$

J_0 is the Bessel function of order zero, and C_2 and C_3 are constants that have to be determined from the boundary conditions. In view of eq A.4, the boundary conditions $\psi_2 = \psi_3$, at $z = 0$, and eq A.3 acquire the form

$$\frac{Q}{\epsilon_2 (r^2 + b^2)^{1/2}} + \tilde{\psi}_2 = \tilde{\psi}_3 \quad (\text{at } z = 0) \quad (\text{A.8})$$

$$\frac{Qb}{(r^2 + b^2)^{3/2}} + \epsilon_2 \frac{\partial \tilde{\psi}_2}{\partial z} = \epsilon_3 \frac{\partial \tilde{\psi}_3}{\partial z} \quad (\text{at } z = 0) \quad (\text{A.9})$$

The first terms in the left-hand side of eqs A.8 and A.9 have the following Hankel transforms:

$$\frac{1}{(r^2 + b^2)^{1/2}} = \int_0^\infty e^{-bk} J_0(kr) dk \quad (\text{A.10})$$

$$\frac{b}{(r^2 + b^2)^{3/2}} = \int_0^\infty e^{-bk} J_0(kr) k dk \quad (\text{A.11})$$

Equation A.11 can be derived by the differentiation of eq A.10 with respect to b . With the help of eqs A.6, A.7, A.10, and A.11, we obtain the Hankel transforms of the boundary conditions, eqs A.8 and A.9:

$$\frac{Q}{\epsilon_2} e^{-bk} + kC_2 = kC_3 \quad (\text{A.12})$$

$$Qe^{-bk} - \epsilon_2 kC_2 = \epsilon_3 qC_3 \quad (\text{A.13})$$

From eqs A.12 and A.13, we determine C_2 and substitute the result into eq A.6:

$$\tilde{\psi}_2 = -\frac{Q}{\epsilon_2} \int_0^\infty \frac{\epsilon_3 q - \epsilon_2 k}{\epsilon_3 q + \epsilon_2 k} e^{-(b+z)k} J_0(kr) dk \quad (\text{A.14})$$

Furthermore, to calculate the force F_z acting on the particle, we have to substitute eq A.4, along with eq A.14, into eq 2.24. The same result can be obtained in the following simpler way: Note that the first term in eq A.4 is the electric potential created by a point charge of magnitude Q situated at $z = b$. The second term in eq A.4 represents the potential created by the image charge. Then, the force of interaction between the original charge Q and the respective image charge is

$$F_z = -Q \frac{\partial \tilde{\psi}_2}{\partial z} \Big|_{r=0, z=b} \quad (\text{A.15})$$

By substitution of eq A.14 into eq A.15 and after some transformations, we obtain

$$F_z = \frac{Q^2}{4\epsilon_2 b^2} B_{23}; \quad B_{23} = \beta_{23}(1 + C_{23}) \quad (\text{A.16})$$

$$C_{23} = \frac{2\epsilon_2}{\epsilon_3 - \epsilon_2} \int_0^\infty \frac{[u^2 + (2\kappa b)^2]^{1/2} - u}{[u^2 + (2\kappa b)^2]^{1/2} + \epsilon_2 u / \epsilon_3} e^{-u} u du \quad (\text{A.17})$$

in which $u = 2\kappa b$. When there is no electrolyte in phase 3, then $\kappa = 0$, $C_{23} = 0$, and $B_{23} = \beta_{23}$. On the other hand, at sufficiently large electrolyte concentrations, we have $2\kappa b \gg 1$. In this limit, for finite u , the fraction in the integrand of eq A.17 is equal to 1, whereas, at greater u , the integrand itself is zero because of the multiplier e^{-u} . Thus, we obtain

$$C_{23} \rightarrow \frac{2\epsilon_2}{\epsilon_3 - \epsilon_2} \int_0^\infty e^{-u} u du = \frac{2\epsilon_2}{\epsilon_3 - \epsilon_2} \quad \text{for } 2\kappa b \rightarrow \infty \quad (\text{A.18})$$

Substituting β_{23} from eq 2.21 and C_{23} from eq A.18 into eq A.16, we obtain $B_{23} = -1$. In this way, we confirm the validity of eq 3.7.

Supporting Information Available: Expression for the electric force acting on the particle (Appendix B) and the recurrence formula for the coefficients A_n (Appendix C). This material is available free of charge via the Internet at <http://pubs.acs.org>.

LA052273J